Caveolin-1 Deficiency Stimulates Neointima Formation during Vascular Injury†

Ghada S. Hassan,‡ Jean-François Jasmin,‡ William Schubert,‡ Philippe G. Frank,‡,§ and Michael P. Lisanti*,‡

Department of Molecular Pharmacology and The Albert Einstein Cancer Center, Albert Einstein College of Medicine, 1300 Morris Park Avenue, Bronx, New York 10461, and Department of Urology, Albert Einstein College of Medicine, 1300 Morris Park, Avenue, Bronx, New York 10461

Received February 25, 2004; Revised Manuscript Received April 30, 2004

ABSTRACT: Neointima formation is a process characterized by smooth muscle cell (SMC) proliferation and extracellular matrix deposition in the vascular intimal layer. Here, we critically evaluate the role of caveolin-1 (Cav-1) in the pathogenesis of neointima formation. Cav-1 and caveolae organelles are particularly abundant in SMCs, where they are thought to function in membrane trafficking and signal transduction events. To directly evaluate the role of Cav-1 in the pathogenesis of neointimal lesions, we used Cav-1-deficient (Cav-1 −/−) mice as a model system. The right common carotid artery of wild-type and Cav-1 −/− mice was ligated just proximal to its bifurcation. Specimens were then harvested 4-weeks postligation and processed for morphometric and immunohistochemical analyses. The carotids of Cav-1 −/− mice showed significantly more intimal hyperplasia with subtotal luminal obstruction, as compared to wild-type mice. These neointimal lesions consisted mainly of SMCs. Mechanistically, neointimal lesions derived from Cav-1 −/− mice exhibited higher levels of phospho-p42/44 MAP kinase and cyclin D1 immunostaining, consistent with the idea that Cav-1 functions as a negative regulator of signal transduction. A significant increase in phospho-Rb (Ser780) immunostaining was also observed, in line with the upregulation of cyclin D1. In conclusion, using a carotid artery blood-flow cessation model, we show that genetic ablation of Cav-1 in mice stimulates SMC proliferation (neointimal hyperplasia), with concomitant activation of the p42/44 MAP kinase cascade and upregulation of cyclin D1. Importantly, our current study is the first to investigate the role of Cav-1 in SMC proliferation in the vascular system using Cav-1 −/− mice.

Neointimal hyperplasia is a signature feature of early atherosclerosis, restenosis after angioplasty, and bypass-graft failure. The events leading to the development of neointimal lesions have been well-studied and include the migration of smooth muscle cells (SMCs)[1] into the intima, followed by proliferation and matrix deposition (*1*). Blood-flow reduction has been shown to increase intimal formation in vascular grafts and balloon-injured vessels, implying that alterations in blood flow affect the proliferative response of SMCs (*2*−*4*). Kumar and Lindner have developed a model in which blood flow in the common carotid artery of the mouse is arrested by carefully ligating the vessel near the bifurcation. In this model, a neointimal lesion develops proximal to the ligation site, as a consequence of partial blood stasis, reduced shear stress, and enhanced arterial wall tension (*5*).

Caveolae are specialized membrane microdomains that function in vesicular and cholesterol trafficking and that have also been implicated in signal transduction at the plasma membrane. Caveolin proteins form a scaffold onto which many classes of signaling molecules can assemble to generate "preassembled" signaling complexes (*6*, *7*). In addition to concentrating these signal transducers within a distinct region of the plasma membrane, caveolin binding may functionally regulate the activation state of these signaling molecules. These caveolin-interacting proteins include endothelial nitric oxide synthase (eNOS), as well as H-Ras and extracellular signal-regulated kinase (ERK-1/2) (*6*−*8*).

Caveolin-1 (Cav-1) is the principal structural protein of caveolae membranes in vascular endothelial cells and SMCs (*9*). Several lines of evidence suggest that Cav-1 plays a negative regulatory role in signaling, i.e., by functioning as a direct inhibitor of a variety of plasma-membrane-initiated signaling cascades (*10*). We and others have recently reported on the generation of Cav-1-deficient (Cav-1 −/−) mice by using standard homologous recombination techniques (*11*−*13*). Interestingly, Cav-1 −/− fibroblasts, adipocytes, endothelial cells, and SMCs (Figure 1) all lack morphologically identifiable caveolae organelles.

The generation of Cav-1-deficient mice by targeted gene deletion has allowed for the exploration of the role of each caveolin gene in the context of a whole organismal model.

† This work was supported by grants from National Institutes of Health (NIH), the Susan G. Komen Breast Cancer Foundation, and the American Heart Association, as well as Hirschl/Weil-Caulier Career Scientist Award (all to M.P.L.). G.S.H. and J.F.J. were recipients of postdoctoral fellowships from the Foundation of Health Research (FRSQ), Quebec, Canada. P.G.F. was the recipient of a Scientist Development Grant from the American Heart Association.

* To whom correspondence should be addressed. Tel: 718-430-8828. Fax: 718-430-8830. E-mail: lisanti@aecom.yu.edu.

‡ Department of Molecular Pharmacology and The Albert Einstein Cancer Center.

§ Department of Urology.

[1] Abbreviations: Cav-1, caveolin-1; EEL, external elastic lamina; eNOS, endothelial nitric oxide synthase; GAPDH, glyceraldehyde-3-phosphate dehydrogenase; H&E, hematoxylin and eosin; IEL, internal elastic lamina; KO, knockout; MAP, mitogen-activated protein; SMCs, smooth muscle cells; WT, wild type.

10.1021/bi049609t CCC: $27.50
Published on Web 06/12/2004

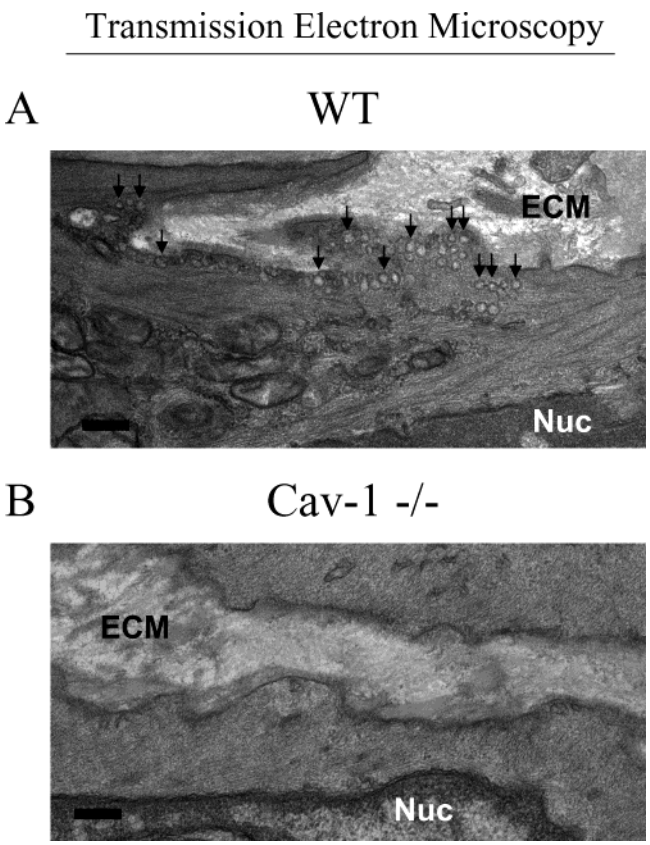

FIGURE 1: Vascular SMCs show a loss of caveolae in Cav-1 (−/−) KO mice, as seen by transmission electron microscopy. Control WT (A) and control Cav-1 −/− (B) nonligated carotid arteries were isolated and processed for electron microscopy. (A) Note that plasmalemmal caveolae are abundant in WT vascular SMCs of the carotid artery (see arrows). (B) In contrast, Cav-1 −/− SMCs of the carotid artery show a specific ablation of caveolae organelles. Bar = 200 nm. ECM, extracellular matrix; Nuc, nucleus.

The first reports on Cav-1 −/− mice describe the hyperproliferation of mouse embryo fibroblasts in culture and lung hypercellularity because of the presence of an increased number of endothelial cells (*11*, *13*), consistent with the idea that Cav-1 normally functions as a negative regulator of cell growth (*14*). Furthermore, we have recently demonstrated that Cav-1 null mice develop mammary epithelial cell hyperplasia, even in 6-week-old virgin mice (*15*). Moreover, Cav-1-deficient mice develop cardiac hypertrophy and show hyperactivation of the Ras-p42/44 MAP kinase cascade in cardiac interstitial fibrotic lesions in vivo. Similarly, hyperactivation of the Ras-p42/44 MAP kinase cascade was observed in isolated cardiac fibroblasts in culture (*16*). Thus, we hypothesize that Cav-1 null mice may possess other hyperproliferative phenotypes.

Here, we investigate the role of Cav-1 in neointima formation by evaluating the influence of targeted deletion of the Cav-1 gene on vascular remodeling after flow cessation in murine carotid arteries. Our results provide the first genetic evidence that Cav-1 negatively regulates SMC proliferation in an in vivo setting.

MATERIALS AND METHODS

Animals. Cav-1 −/− mice were generated as previously described (*12*). All animals used in the current studies were in the C57BL/6J genetic background and were genotyped by polymerase chain reaction, as previously described (*12*). Housing and maintenance were provided by the Albert Einstein College of Medicine barrier facility. Mice were kept on a 12-h light/dark cycle and had ad libitum access to food and water. All animal protocols used in this study were preapproved by the Albert Einstein College of Medicine—Institute for Animal Studies. Cav-1 −/− mice, 12−16 weeks of age ($n = 7$), and sex-, age-, and strain-matched (C57BL/6J) wild-type (WT) littermates ($n = 9$) were used.

Electron Microscopy. Murine carotid arteries were isolated and fixed with 2.5% glutaraldehyde/0.1 M cacodylate, postfixed with OsO_4, and stained with uranyl acetate and lead citrate. Samples were then examined under a JEOL 1200EX transmission electron microscope and photographed at a magnification of 25 000×. SMC caveolae were identified by their characteristic flask shape, size (50−100 nm), and location at or near the plasma membrane (*12*).

Flow Cessation Model. The carotid artery ligation model used in our experiments has been previously described (*5*). Briefly, WT and Cav-1 −/− mice were anesthetized by intraperitoneal injection of ketamine HCl and xylazine (80 and 5 mg/kg body weight, respectively). The right common carotid artery was dissected and ligated just proximal to its bifurcation with a 6−0 silk ligature. The animals were processed for morphological and biochemical studies at 4 weeks after the initial surgery.

Histology and Morphometry. Mice were euthanized and transcardially perfused with 4% paraformaldehyde in phosphate-buffered saline (PBS) under physiological pressure. Fixed ligated arteries were embedded in paraffin. For the morphometric analysis, sections (5-μm thick) at 2 mm proximal to the ligated site were stained with hematoxylin and eosin (H&E). Digital microscopic images were analyzed using the image analysis software, NIH Image J. Perimeters of the lumen, the internal elastic lamina (IEL), and the external elastic lamina (EEL) were obtained by tracing the contours on digitized images. The intimal and medial areas were calculated by subtracting the area defined by the lumen from the area defined by the IEL and subtracting the area defined by the IEL from the area defined by the EEL. The neointimal area was determined by subtracting the lumenal area from the area defined by the IEL. For the evaluation of collagen deposition, Masson's Trichrome staining was performed on proximal sections.

Immunohistochemical Techniques. Paraffin (5 μm) sections were immunostained with antibodies directed against SMC-α-actin (DAKO, clone 1A4), proliferating cell nuclear antigen (PCNA, BD Pharmingen, San Diego, CA), phospho-ERK-1/2 (pERK, Cell Signaling Technology, Beverly, MA), cyclin D1 (NeoMarkers, Fremont, CA), phospho-Rb (pRb-Ser780, Cell Signaling Technology, Beverly, MA), and $p21^{Cip1/Waf1}$ (p21-C-19, Santa Cruz Biotechnology, Santa Cruz, CA) using the avidin-biotin peroxidase method. In brief, paraffin sections were dewaxed in xylene for 20 min, rehydrated in alcohol, and washed in PBS, and then all sections were incubated with Triton-X 100 (0.2%) for 30 min. After 3 washes with PBS, they were incubated for 30 min with 5% H_2O_2 to block endogenous peroxidase activity, incubated with 10% normal goat serum for 30 min, and then incubated with the corresponding primary antibody for 18 h at 4 °C. Next, sections were incubated with biotinylated IgG (1:200) for 45 min and stained using the immunoperoxidase

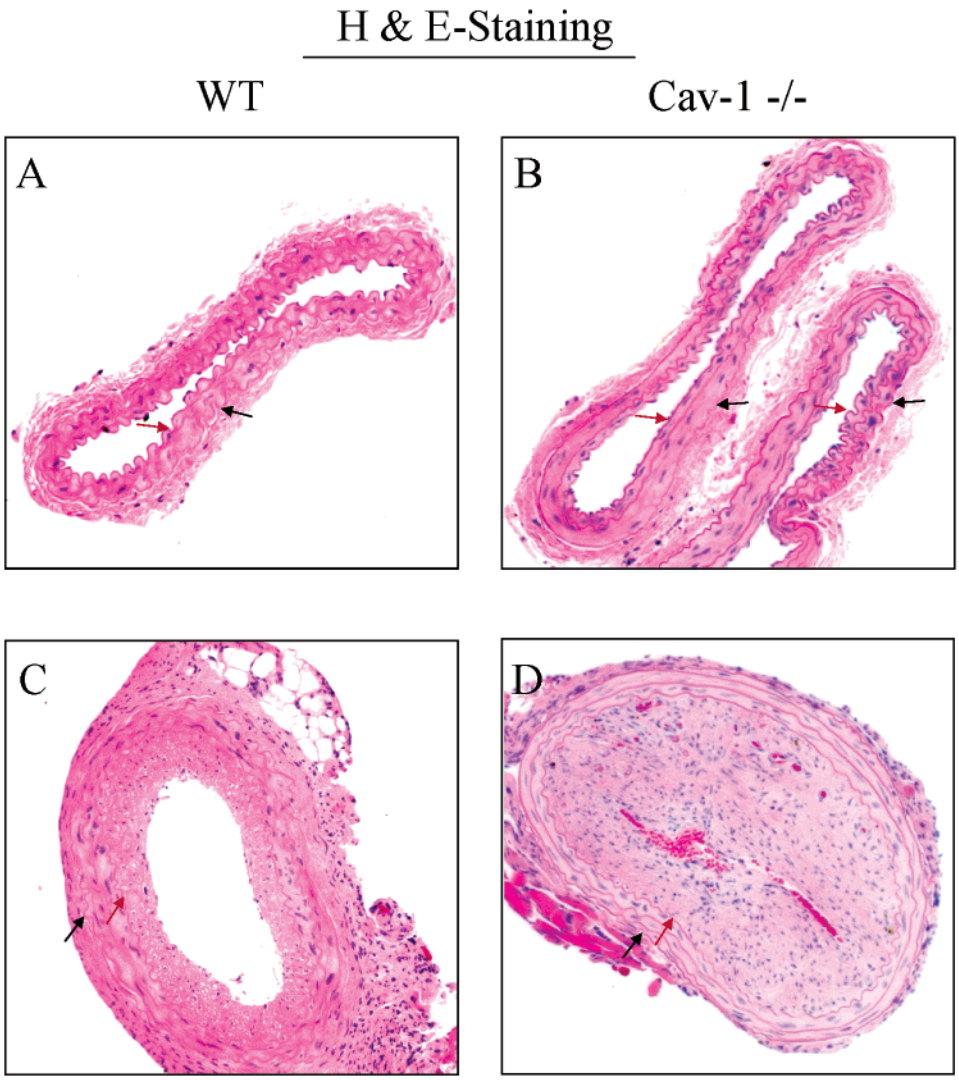

FIGURE 2: Histological analysis of WT and Cav-1 −/− carotid arteries retrieved 4-weeks postligation. (A and B) H&E staining of control WT (A) and control Cav-1 −/− (B) nonligated arteries. Note that both WT and Cav-1 −/− carotid arteries appear normal, without any evidence of baseline SMC hyperproliferation or migration. (C and D) H&E staining of ligated WT (C) and ligated Cav-1 −/− (D) arteries. Note that the carotids of Cav-1 −/− mice show significantly more intimal hyperplasia with subtotal luminal obstruction, as compared to WT mice. In A−D, red arrows denote the IEL and black arrows denote the EEL.

technique, according to the instructions of the manufacturer (Vectastain ABC Elite Kit, Vector Laboratories, Burlingame, CA) for 45 min at room temperature. The sections were developed using diaminobenzidine (DAB) and hydrogen peroxide, then counterstained with hematoxylin, dehydrated, and cleared. Finally, glass cover slips were placed on top of the sections. Negative controls were performed to rule out nonspecific staining, such as secondary alone, and the use of nonimmune serum in place of the primary antibody.

Statistical Analysis. Values are reported as the mean ± standard error of the mean (SEM). Comparisons between Cav-1 −/− and WT mice were performed using a one way analysis of variance (ANOVA) and the Student *T* test, where appropriate.

Tissue Preparation and Western Blot Analysis of the Aorta. After the mice were killed by CO_2 asphyxiation, aortas were collected from the heart to the iliac bifurcation and dissected to remove any adventitial tissue. After a short wash in PBS, aortas were snap frozen in liquid nitrogen. Samples were then homogenized in 5 volumes of boiling lysis buffer (1% sodium dodecyl sulfate (SDS), 1.0 mM sodium-orthovanadate, and 10 mM Tris at pH 7.4). Homogenates were further sonicated and then centrifuged at 16000*g* at 4 °C for 10 min to pellet insoluble material. Protein concentrations were measured with the bicinchoninic acid protein assay (Bio-Rad Laboratories), with bovine serum albumin as the protein standard. Equal amounts of protein for each sample were loaded and run on SDS−PAGE 12% gels. After the transfer to nitrocellulose, the activation state and expression levels of several signal transducers (PCNA, cyclin D1, ERK-1/2, Rb, and $p21^{Cip1/Waf1}$) were examined by using specific antibodies. Antibodies directed against glyceraldehyde-3-phosphate dehydrogenase (GAPDH, Research Diagnostics, Inc.) were used as a control for equal loading.

RESULTS

Vascular SMCs Show a Loss of Caveolae in Cav-1 Knockout (KO) Mice. Caveolae organelles are particularly abundant in SMCs and are formed by the oligomerization of the caveolin proteins. As such, we first examined the status of caveolae formation in vascular SMCs in the carotid arteries of WT and Cav-1 −/− mice.

Ablation of Cav-1 gene expression was sufficient to essentially eliminate caveolae formation in vascular SMCs. Figure 1 shows that plasmalemmal caveolae are especially numerous in WT vascular SMCs of the carotid artery; in contrast, Cav-1 −/− SMCs conspicuously lack caveolae organelles.

Thus, loss of Cav-1 prevents caveolae formation in vascular SMCs in vivo. Importantly, these data are consistent with our previous results obtained using Cav-1 −/− bladder smooth muscle (*22*).

A Cav-1 Deficiency (−/−) Dramatically Stimulates Neointima Formation. The changes in vessel wall geometry in response to flow reduction in WT and Cav-1 −/− mice were determined by measuring the luminal, intimal, and medial areas of carotid arteries after vessel ligation. Lesion development was assessed 4 weeks after ligation, at which time the lesion is fully established (*5*).

In WT mice, 4 weeks after ligation, a neointimal lesion, 4−6 cell layers thick, was observed in the area proximal to the ligation (Figure 2), similar to what has been reported by other laboratories (*5*, *17*, *18*). This resulted in an intimal/medial ratio of 1.1 ± 0.3 as compared to 0.1 ± 0.01 in control nonligated arteries, $p < 0.01$ (Figure 3).

Importantly, in the Cav-1 null mouse, ligation of the common carotid artery caused a significant increase in neointimal lesion development compared to WT mice (Figures 2 and 3). This change was exemplified by a greater than 2-fold increase in the intimal/medial ratio (2.4 ± 0.3, Figure 3). This increase was mostly due to a significant change in the intimal area, which increased ∼2−3-fold in the Cav-1 −/− mice, as compared to the WT mice (33 942 ± 3944 μm^2 versus 14 668 ± 3473 μm^2, respectively, $p < 0.001$, Figure 2).

A small but statistically significant increase in the medial area was also observed in Cav-1 −/− (14 584 ± 1128 μm^2) and WT ligated arteries (13 332 ± 852 μm^2) compared to the nonligated controls (10 517 ± 978 μm^2 and 7552 ± 321 μm^2, respectively); this might cause an underestimate of the intimal/medial ratio observed in the ligated arteries. Importantly, the contralateral carotid artery, used as a control in each animal, showed no neointimal formation.

Therefore, neointima formation, which occurred as a response to the loss of net flow was much more extensive in Cav-1 −/− mice than in WT mice. These results indicate that, in a flow-restricted carotid artery, Cav-1 expression normally negatively regulates neointimal development, such that, in the case of a Cav-1 deficiency, lesion size is dramatically increased.

Neointimal Lesions Are Composed of SMCs and Extracellular Matrix. The cellular composition of neointimal lesions was determined by immunological and histochemical methods. Immunostaining with anti-SMC-α-actin IgG revealed that SMCs were the major component of neointimal lesions in both Cav-1 −/− and WT mice (Figure 4). The neovascularization formed in the intimal thickening also showed SMC-α-actin immunopositive cells. The presence of monocytes/macrophages and other leukocytes was also investigated using an antibody directed against leukocyte common antigen (LCA). However, few or no leukocytes were present in the neointimal lesions in Cav-1 −/− or WT mice (data not shown). Moreover, collagen deposition was significantly noted in lesions of both groups (Figure 4).

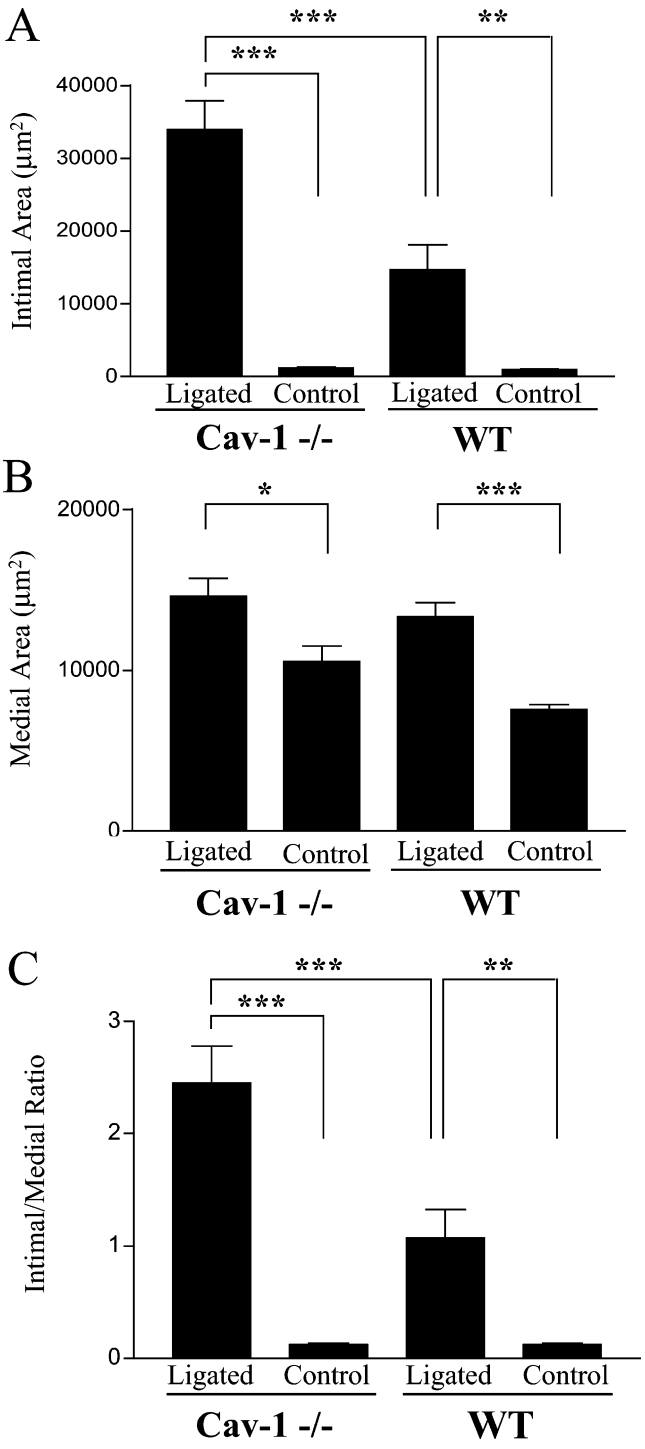

FIGURE 3: Morphometric analysis of neointima formation in WT and Cav-1 −/− mice. Changes in vessel wall geometry in response to flow reduction in WT and Cav-1 −/− mice were determined by measuring the luminal, intimal, and medial areas of carotid arteries after vessel ligation. Digital microscopic images were analyzed using the image analysis software, NIH Image J (see the Materials and Methods). The (A) intimal area, (B) medial area, and (C) intimal/medial ratio are shown. Note that, in Cav-1 −/− mice, ligation of the common carotid artery caused a significant increase in neointimal lesion development. This increase was mostly due to a significant increase in the intimal area, which increased ∼2−3-fold in Cav-1 −/− mice compared to WT mice (33 942 ± 3944 μm^2 versus 14 668 ± 3473 μm^2, respectively, $p < 0.001$). Cav-1 −/− mice, 12−16 weeks of age ($n = 7$), and sex-, age-, and strain-matched (C57BL/6J) WT littermates ($n = 9$) were used. Data represent the mean ± SEM. Single, double, and triple asterisks indicate $p < 0.05$, $p < 0.01$, and $p < 0.001$, respectively.

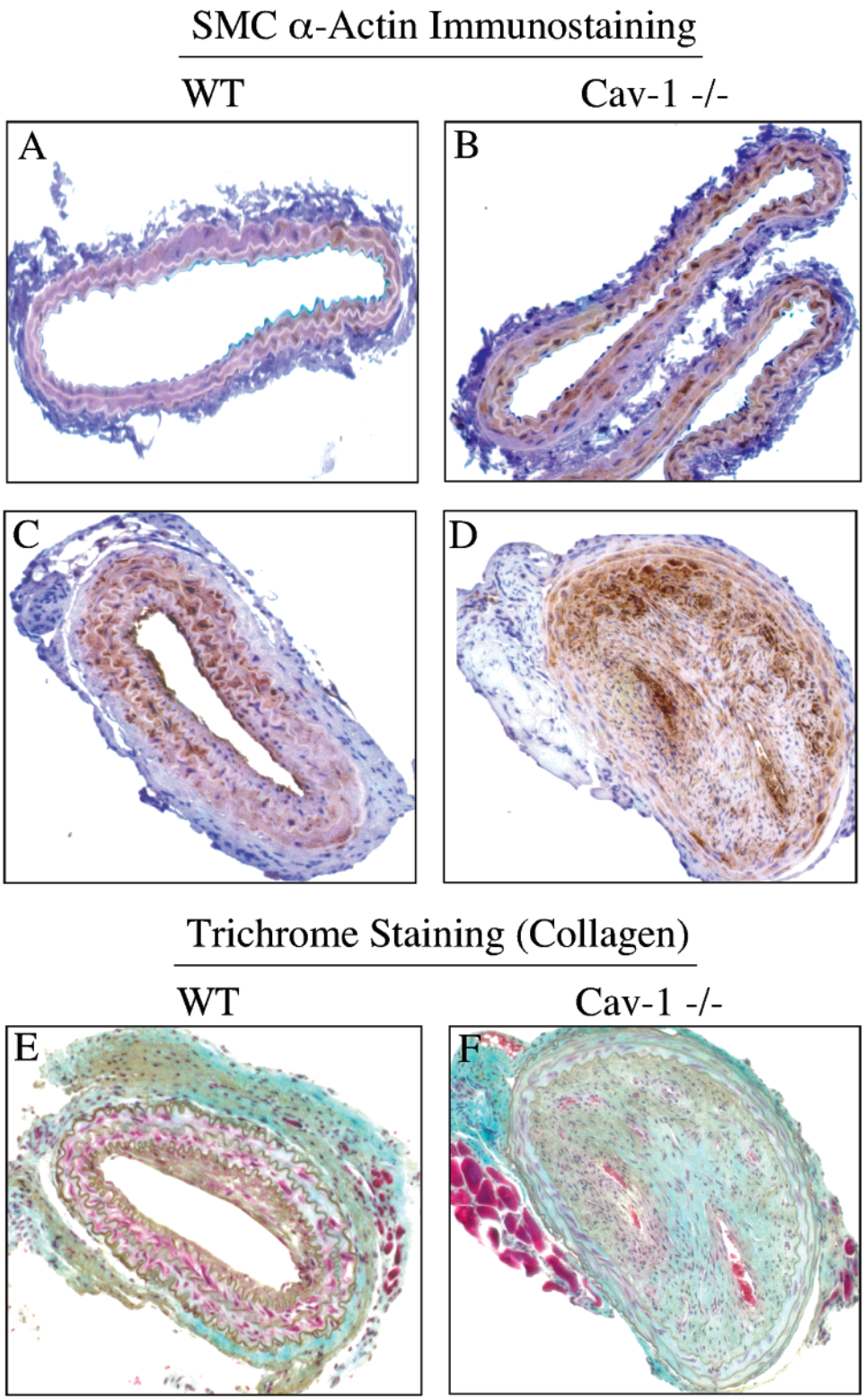

FIGURE 4: Neointimal lesions are composed of SMCs and extracellular matrix in WT and Cav-1 −/− carotid arteries, retrieved 4-weeks postligation. (A and B) Immunostaining with anti-SMC α-actin in control WT (A) and control Cav-1 −/− (B) nonligated carotid arteries. (C and D) Immunostaining with anti-SMC α-actin in ligated WT (C) and ligated Cav-1 −/− (D) carotid arteries. (E and F) Masson's Trichrome staining for collagen deposition in ligated WT (E) and ligated Cav-1 −/− (F) carotid arteries. In A−D, sections were developed using DAB and hydrogen peroxide and then counterstained with hematoxylin.

In addition, we evaluated the proliferation of neointimal cells using a monoclonal antibody directed against PCNA. Interestingly, the mean percentage of PCNA-positive cells was ~2-fold higher in the intimal lesions of Cav-1 −/− mice than in those of their WT counterparts (14.4 ± 3.7% versus 6.7 ± 2.1%, respectively, $p < 0.05$, Figure 5).

Cav-1 −/− Neointimal Lesions Show an Upregulation of Activated ERK-1/2 (p42/44 MAP Kinase) and Cyclin D1 Expression. We next examined the state of vascular signaling in ligated carotid artery cross sections derived from Cav-1 −/− and WT mice. More specifically, using an immunohistochemical approach with antibodies directed against

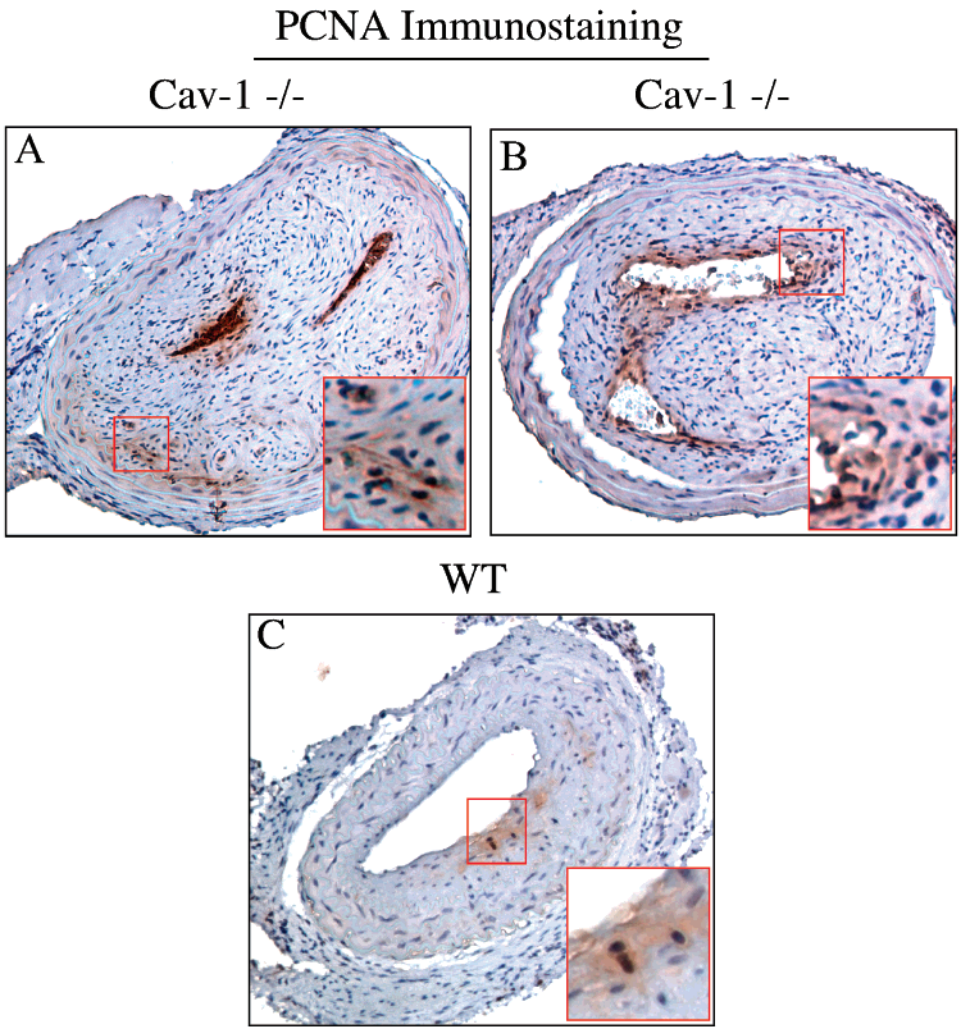

FIGURE 5: Immunohistochemical analysis of the proliferative marker, PCNA, in WT and Cav-1 −/− carotid arteries, at 4-weeks postligation. Note that PCNA nuclear staining was more frequent in the neointimal lesions of Cav1 −/− mice (A and B), as compared to WT lesions (C). Boxed areas (in red) are shown as insets at higher magnification.

phospho-p42/44 MAP kinase (ERK-1/2), cyclin D1, phospho-Rb (Ser780), and $p21^{Cip1/Waf1}$, we evaluated the levels of these signal transducing molecules in Cav-1 −/− versus WT neointimal lesions.

Figure 6 shows that neointimal lesions derived from Cav-1 −/− mice clearly have increased levels of activated ERK-1/2 as compared to WT mice. Similarly, cyclin D1 expression levels were more pronounced in Cav-1 −/− intimal lesions, as well as in medial SMCs, compared to their WT counterparts (Figure 6).

Rb inactivation normally occurs through its phosphorylation on Ser780 by the cyclin D1−cdk4/6 complex, thus, driving cell-cycle progression. As a consequence, we also examined the levels of phospho-Rb (Ser780) by immunostaining. Interestingly, Cav-1 −/− lesions exhibited stronger levels of pRb phosphorylated at Ser780, as compared to WT neointimal lesions (Figure 7). This is consistent with the notion that upregulation of cyclin D1 levels is predicted to increase the phosphorylation of pRb on Ser780.

In addition, in both groups (WT and Cav-1 −/−), ligated arteries always showed higher levels of these three signal transducers (phospho-ERK-1/2, cyclin D1, and phospho-Rb) compared to contralateral nonligated control arteries (data not shown).

Finally, sections from Cav-1 −/− and WT ligated arteries were also checked for $p21^{Cip1/Waf1}$ levels. In contrast, this tumor-suppressor protein was similarly expressed in both WT and Cav-1 −/− neointimal lesions (Figure 7).

Cav-1 Deficiency Alters the Activation State and Expression of Various Signal Transducers in the Vasculature. To facilitate biochemical manipulations and to confirm our results from the immunocytochemistry of carotid arteries, we next harvested the aortas from WT and Cav-1 −/− mice and subjected them to Western blot analysis with antibodies directed against signal transducing molecules. Interestingly, we have previously shown that the aortas of Cav-1 −/− are morphologically normal, as assessed by H&E staining (*12*).

Figure 8 shows that the levels of PCNA, phospho-ERK-1/2, and cyclin D1 (all proproliferative markers) are clearly increased in Cav-1 −/− aortic samples, as compared with WT control mice. Similarly, in Cav-1 −/− aortas, phospho-Rb is also increased in accordance with elevated cyclin D1 expression. In contrast, the levels of $p21^{Cip1/Waf1}$ are considerably reduced. However, the levels of total ERK-1/2 and total Rb remain virtually unchanged. Also, we evaluated the expression of GAPDH as a control for equal loading, and its levels are equivalent in WT and Cav-1 −/− aortic samples.

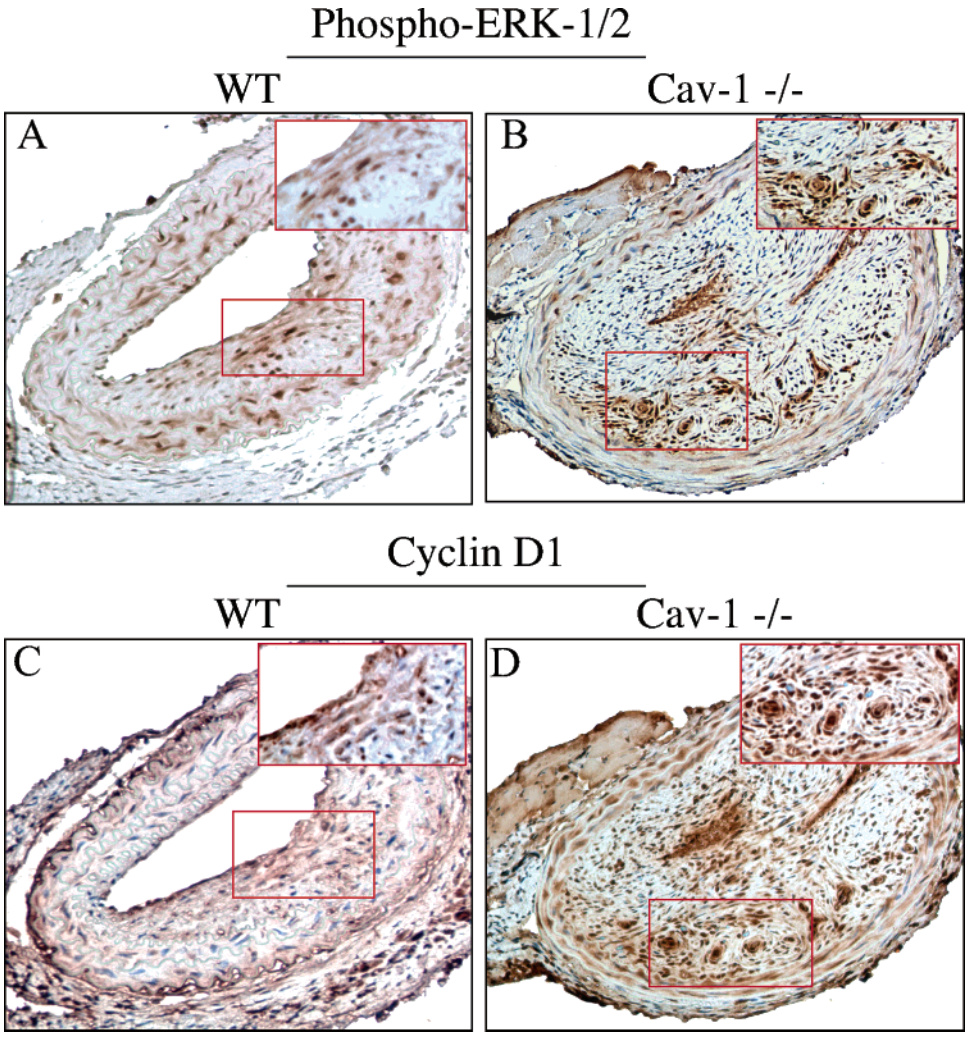

FIGURE 6: Immunohistochemical analysis of phospho-ERK-1/2 and cyclin D1 in WT and Cav-1 −/− carotid arteries, at 4-weeks postligation. (A and B) Activated ERK-1/2. Note that phospho-ERK-1/2 immunostaining was more pronounced in Cav-1 −/− neointimal lesions (B) than in the corresponding WT lesions (A). (C and D) Cyclin D1. Note that cyclin D1 immunostaining was clearly more intense in the Cav-1 −/− neointimal lesions (D) than in the corresponding WT lesions (C). Boxed areas (in red) are shown as insets at higher magnification.

Thus, these biochemical data provide direct support for our findings from the immunocytochemical analysis of carotid artery neointimal lesions. In addition, they suggest a possible molecular basis for the increased predisposition toward neointimal hyperplasia that we observe in Cav-1 −/− mice, given an appropriate stimulus.

DISCUSSION

In this study, we have assessed the proposed role of Cav-1 as a negative regulator of cell proliferation by using genetically engineered mice that harbor a targeted disruption of the Cav-1 locus. We subjected these Cav-1 −/− mice (and their WT littermates) to an interruption of blood flow induced by carotid artery ligation. Then, we quantitatively monitored neointimal formation and evaluated the levels of candidate signal transducing molecules that may be affected by a loss of Cav-1. Interestingly, Cav-1 −/− mice showed a dramatic reduction in luminal area secondary to marked neointimal hyperplasia, consisting mainly of SMCs. Mechanistically, immunohistochemical analysis of these Cav-1 −/− neointimal vascular lesions revealed higher levels of phospho-ERK-1/2, cyclin D1, and phospho-Rb compared to those of the WT mice.

Numerous studies have suggested a role for Cav-1 in cell proliferation and epithelial hyperplasia. Thus, Cav-1 −/− cells are predicted to exhibit derangements in proliferation and/or growth. Indeed, an analysis of the growth properties of primary cultures of mouse embryo fibroblasts (MEFs) reveals that Cav-1 −/− cells display more active cell-cycle profiles than their WT counterparts (a ∼30% increase in the S-phase fraction) and they attain nearly 3-fold higher monolayer densities over a 10-day period (*19*). Moreover, Cav-1 null mice exhibit initial or induced hyperplasia in various cell types, such as cardiac fibroblasts, mammary epithelial cells, and keratinocytes (*16*, *20*, *21*). Regarding SMCs, however, only the bladders of aged male Cav-1 −/− (1-year-old mice) were evaluated and showed a gradual thickening of the smooth muscle layer (*22*). In contrast, no bladder thickening was observed in young Cav-1 −/− (4-months-old mice of either sex) or in aged female Cav-1 −/− mice. Thus, we chose to evaluate young Cav-1 −/− (3−4-month-old mice) in the current study of neointimal hyperplasia. Importantly, our study is the first to investigate the role of Cav-1 in SMC proliferation in the vascular system using Cav-1 −/− mice.

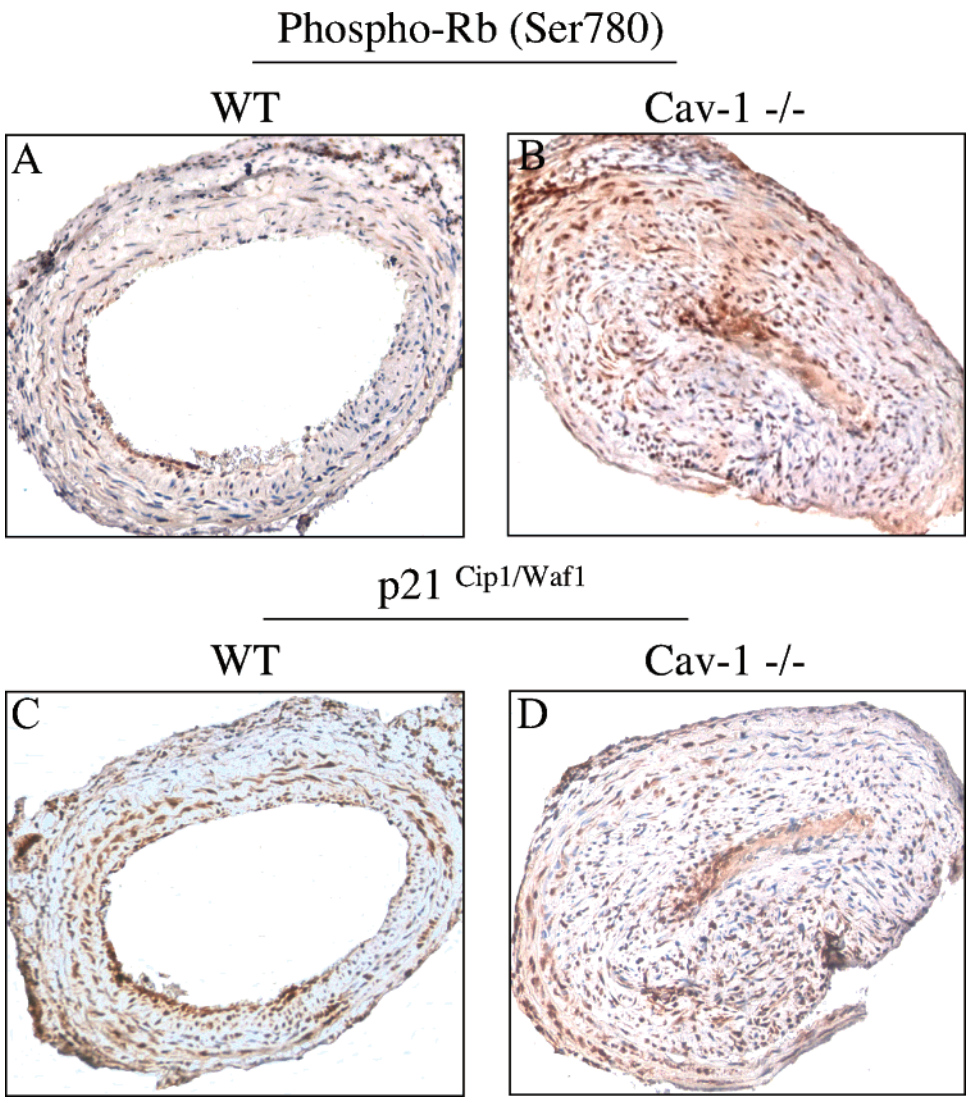

FIGURE 7: Immunohistochemical analysis of phospho-Rb (Ser780) and $p21^{Cip1/Waf1}$ in WT and Cav-1 −/− carotid arteries, at 4-weeks postligation. (A and B) Phospho-Rb (Ser780). Note that immunostaining for the retinoblastoma protein phosphorylated at Ser780 was clearly more pronounced in Cav-1 −/− carotid arteries (B) than in WT arteries (A). (C and D) $p21^{Cip1/Waf1}$. Interestingly, the level of p21 immunostaining was similar in both Cav-1 −/− (D) and WT (C) carotid arteries.

In this report, we have used a model developed by Kumar and Lindner (1997), for studying vascular remodeling in the mouse (*5*). Interruption of blood flow caused by ligating the common carotid artery induces the migration of SMCs from the media to the intima and their proliferation in the intima, leading to neointima formation. Our results show that the ablation of Cav-1 gene expression dramatically increases the size and extent of SMC-rich neointimal lesions induced by blood-flow interruption. This is consistent with the notion that Cav-1 and caveolae organelles normally function to negatively regulate SMC proliferation.

The neointimal region was composed predominantly of SMCs (as revealed by immunohistochemical analysis), with accompanying extracellular matrix (collagen deposition). Vascular cell proliferation, as assessed using antibodies directed against PCNA, was more pronounced in Cav-1 −/− mice, as compared to their WT counterparts. However, the medial thickness observed in ligated vessels compared to the contralateral nonligated arteries control did not differ between WT and Cav-1 −/− mice.

How does Cav-1 regulate cell proliferation? It appears that caveolin binding serves to inhibit multiple parallel downstream signaling events. For example, Cav-1 has been shown to interact with and suppress the kinase activity of the EGF receptor and several members of the Ras-p42/44 MAP kinase cascade, including MEK and ERK, in vitro (*23*, *24*). Conversely, downregulation of Cav-1 in NIH 3T3 fibroblasts (using an antisense cDNA approach) results in hyperactivation of the p42/44 MAP kinase cascade and cellular transformation (*25*). Moreover, downregulation of Cav-1 expression by RNAi in *Caenorhabditis elegans* results in hyperactivation of the meiotic cycle, which is controlled by the Ras-MAP kinase pathway (*26*). Finally, Cav-1 null keratinocytes exhibited increased levels of phospho-ERK-1/2 immunostaining during DMBA-induced epidermal hyperplasia (*21*). In accordance with these findings, we show here that phospho-ERK-1/2 levels are upregulated in Cav-1 −/− neointimal lesions, following blood-flow cessation. Thus, these results provide the first evidence that Cav-1 negatively regulates SMC proliferation in an in vivo setting.

Another possible mechanism by which Cav-1 could regulate cell proliferation is through the upregulation of cyclin D1 expression levels. The cyclin D1 protein is the regulatory component of the holoenzyme that inactivates the

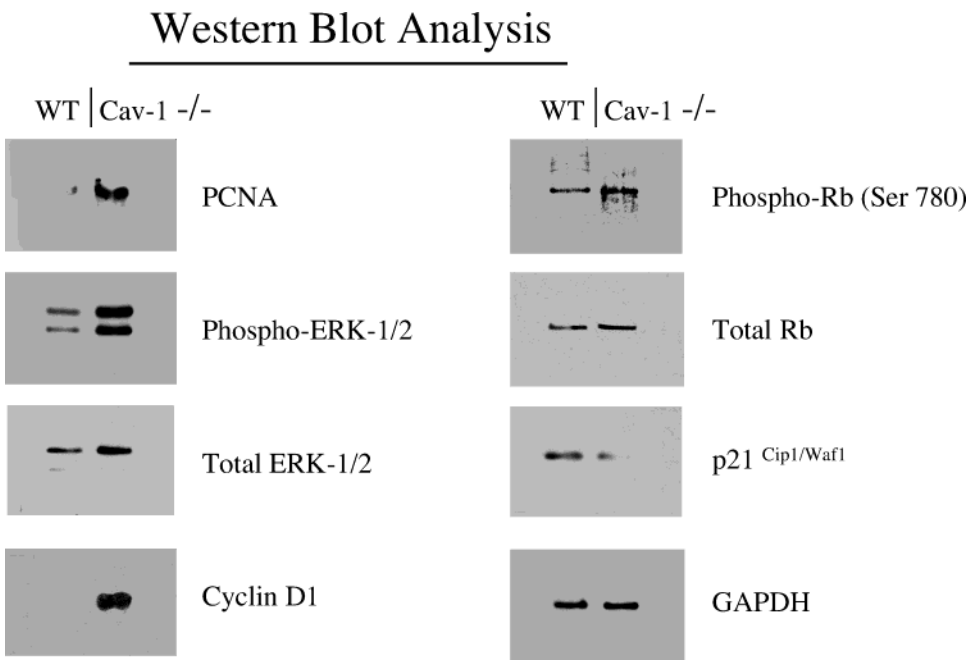

FIGURE 8: Biochemical analysis of the vasculature in WT and Cav-1 −/− mice. Aortas were harvested from WT and Cav-1 −/− mice. After solubilization, equivalent amounts of total protein were then separated by SDS−PAGE and transferred to nitrocellulose. The activation state and expression levels of various signal transducers were assessed with specific antibodies. Note that PCNA, cyclin D1, activated ERK-1/2 (phospho-ERK-1/2), and activated Rb [phospho-Rb (Ser 780)] levels are all upregulated in Cav-1 −/− aortas, as compared to WT controls, consistent with a predisposition toward hyperproliferation. On the other hand, Cav-1 −/− aortas show reduced levels of $p21^{Cip1/Waf1}$. Antibodies directed against GAPDH were used as a control for equal loading.

retinoblastoma pRb protein, implying a role for cyclin D1 in cellular proliferation and tranformation (*27*). D-cyclins are involved in controlling cell-cycle progression by activating their associated kinases, cdk4 and cdk6. These cyclin-dependent kinases phosphorylate the retinoblastoma pRb protein, leading to transition through the G1 phase of the cell cycle (*28*). We have shown that overexpression of Cav-1 causes transcriptional repression of cyclin D1, whereas expression of antisense Cav-1 increases cyclin D1 levels, in cultured cell models (*27*). In the present study, we show here that cyclin D1 is upregulated in the neointimal region of Cav-1 −/− arteries following blood interruption, lending further support to the idea that Cav-1 performs a negative growth regulatory function. Furthermore, our results also showed increased levels of the retinoblastoma protein, the substrate of the cyclin-D−cdk4/6 complex, phosphorylated at Ser780. The phosphorylation of Rb at Ser780 is induced specifically by the cyclin D1−cdk4 complex and not the cyclin E−cdk-2 complex and inhibits the binding of pRb to E2F-1 (*29*). This process induces cell-cycle progression. Moreover, several studies have reported enhanced phosphorylation of pRb associated with an overexpression of cyclin D1 in proliferating SMCs (*30*−*32*). Therefore, our findings suggest a mechanism involving the hyperactivation of SMC proliferation mediated through the Ras-p42/44 MAP kinase and the cyclin D1−phospho-Rb pathways.

In addition to the cdk-activator, cyclin D1, we investigated the expression levels of $p21^{Cip1/Waf1}$, a cdk inhibitor. Cho et al. have shown that a reduction in the levels of Cav-1 using antisense oligonucleotides and small interfering RNA, decreased the level of $p21^{Cip1/Waf1}$ in epidermal growth-factor-stimulated fibroblasts (*33*). However, in our study, deletion of the Cav-1 gene did not appear to dramatically alter $p21^{Cip1/Waf1}$ levels in arteries with neointimal formation, as seen by immunocytochemistry. In contrast, we observed a clear downregulation of $p21^{Cip1/Waf1}$ levels by Western blot analysis. This minor discrepancy may be due to the increased sensitivity afforded by immunoblotting. Thus, $p21^{Cip1/Waf1}$ levels are indeed affected in the vasculature of Cav-1 −/− mice, consistent with the above-noted Cav-1 antisense studies (*33*).

Besides regulating cell proliferation, Cav-1 has also been shown to affect the migration of epithelial cells. Recombinant expression of Cav-1 in MTLn3, a metastatic rat mammary adenocarcinoma cell line, inhibits EGF-stimulated lamellipod extension and cell migration, probably through inhibition of the p42/44 MAP kinase cascade (*34*). In the present study, the absence of Cav-1 gene expression increased neointimal formation, characterized by SMC migration and proliferation. Thus, loss of Cav-1 could play a role not only in stimulating SMC proliferation, but also in enhancing SMC migration from the media to the intimal layer.

In conclusion, our results indicate that Cav-1 plays an important in vivo role in suppressing the proliferation and/or migration of vascular SMCs. As such, an absence of Cav-1 facilitates the appearance of neointimal lesions that are clinically relevant to the pathogenesis of many vascular diseases, including restenosis after angioplasty and bypass-graft failure. Therefore, our current findings identify Cav-1 and caveolae organelles as novel targets for drug development to pharmacologically prevent the formation of neointimal vascular lesions.

ACKNOWLEDGMENT

We especially thank Dr. Federica Sotgia for her expert intellectual and technical advice. We also thank Dr. Radma Mahmood and Mr. Victor Nieves (from the Histotechnology and Comparative Pathology Facility at Einstein) for their help with carotid artery tissue processing, embedding, and sectioning.

REFERENCES

1. Ross R. (1993) The pathogenesis of atherosclerosis: A perspective for the 1990s, *Nature 362*, 801−809.
2. Bassiouny, H. S., White, S., Glagov, S., Choi, E., Giddens, D. P., and Zarins, C. K. (1992) Anastomotic intimal hyperplasia: Mechanical injury or flow induced, *J. Vasc. Surg. 15*, 708−717.
3. Geary, R. L., Kohler, T. R., Vergel, S., Kirkman, T. R., and Clowes, A. W. (1994) Time course of flow-induced smooth muscle cell proliferation and intimal thickening in endothelialized baboon vascular grafts, *Circ. Res. 74*, 14−23.
4. Kohler, T. R., Kirkman, T. R., Kraiss, L. W., Zierler, B. K., and Clowes, A. W. (1991) Increased blood flow inhibits neointimal hyperplasia in endothelialized vascular grafts, *Circ. Res. 69*, 1557−1565.
5. Kumar, A., and Lindner, V. (1997) Remodeling with neointima formation in the mouse carotid artery after cessation of blood flow, *Arterioscler., Thromb., Vasc. Biol. 17*, 2238−2244.
6. Razani, B., Woodman, S. E., and Lisanti, M. P. (2002) Caveolae: From cell biology to animal physiology, *Pharmacol. Rev. 54*, 431−467.
7. Razani, B., and Lisanti, M. P. (2001) Caveolin-deficient mice: Insights into caveolar function and human disease, *J. Clin. Invest. 108*, 1553−1561.
8. Smart, E. J., Graf, G. A., McNiven, M. A., Sessa, W. C., Engelman, J. A., Scherer, P. E., Okamoto, T., and Lisanti, M. P. (1999) Caveolins, liquid-ordered domains, and signal transduction, *Mol. Cell. Biol. 19*, 7289−7304.
9. Scherer, P. E., Lewis, R. Y., Volonte, D., Engelman, J. A., Galbiati, F., Couet, J., Kohtz, D. S., van Donselaar, E., Peters, P., and Lisanti, M. P. (1997) Cell-type and tissue-specific expression of caveolin-2. Caveolins 1 and 2 co-localize and form a stable hetero-oligomeric complex in vivo, *J. Biol. Chem. 272*, 29337−29346.
10. Okamoto, T., Schlegel, A., Scherer, P. E., and Lisanti, M. P. (1998) Caveolins, a family of scaffolding proteins for organizing "pre-assembled signaling complexes" at the plasma membrane, *J. Biol. Chem. 273*, 5419−5422.
11. Razani, B., Engelman, J. A., Wang, X. B., Schubert, W., Zhang, X. L., Marks, C. B., Macaluso, F., Russell, R. G., Li, M., Pestell, R. G., Di Vizio, D., Hou, H., Jr, Kneitz, B., Lagaud, G., Christ, G. J., Edelmann, W., and Lisanti, M. P. (2001) Caveolin-1 null mice are viable but show evidence of hyperproliferative and vascular abnormalities, *J. Biol. Chem. 276*, 38121−38138.
12. Schubert, W., Frank, P. G., Razani, B., Park, D. S., Chow, C. W., and Lisanti, M. P. (2001) Caveolae-deficient endothelial cells show defects in the uptake and transport of albumin in vivo, *J. Biol. Chem. 276*, 48619−48622.
13. Drab, M., Verkade, P., Elger, M., Kasper, M., Lohn, M., Lauterbach, B., Menne, J., Lindschau, C., Mende, F., Luft, F. C., Schedl, A., Haller, H., and Kurzchalia, T. V. (2001) Loss of caveolae, vascular dysfunction, and pulmonary defects in caveolin-1 gene-disrupted mice, *Science 293*, 2449−2452.
14. Galbiati, F., Volonte, D., Liu, J., Capozza, F., Frank, P. G., Zhu, L., Pestell, R. G., and Lisanti, M. P. (2001) Caveolin-1 expression negatively regulates cell cycle progression by inducing G(0)/G(1) arrest via a p53/p21(WAF1/Cip1)-dependent mechanism, *Mol. Biol. Cell 12*, 2229−2244.
15. Lee, H., Park, D. S., Razani, B., Russell, R. G., Pestell, R. G., and Lisanti, M. P. (2002) Caveolin-1 mutations (P132L and null) and the pathogenesis of breast cancer: Caveolin-1 (P132L) behaves in a dominant-negative manner and caveolin-1 (−/−) null mice show mammary epithelial cell hyperplasia, *Am. J. Pathol. 161*, 1357−1369.
16. Cohen, A. W., Park, D. S., Woodman, S. E., Williams, T. M., Chandra, M., Shirani, J., Pereira de Souza, A., Kitsis, R. N., Russell, R. G., Weiss, L. M., Tang, B., Jelicks, L. A., Factor, S. M., Shtutin, V., Tanowitz, H. B., and Lisanti, M. P. (2003) Caveolin-1 null mice develop cardiac hypertrophy with hyperactivation of p42/44 MAP kinase in cardiac fibroblasts, *Am. J. Physiol. 284*, C457−C474.
17. Harmon, K. J., Couper, L. L., and Lindner, V. (2000) Strain-dependent vascular remodeling phenotypes in inbred mice, *Am. J. Pathol. 156*, 1741−1748.
18. Kraemer, R. (2002) Reduced apoptosis and increased lesion development in the flow-restricted carotid artery of p75(NTR)-null mutant mice, *Circ. Res. 91*, 494−500.
19. Razani, B., Altschuler, Y., Zhu, L., Pestell, R. G., Mostov, K. E., and Lisanti, M. P. (2000) Caveolin-1 expression is down-regulated in cells transformed by the human papilloma virus in a p53-dependent manner. Replacement of caveolin-1 expression suppresses HPV-mediated cell transformation, *Biochemistry 39*, 13916−13924.
20. Williams, T. M., Cheung, M. W., Park, D. S., Razani, B., Cohen, A. W., Muller, W. J., Di Vizio, D., Chopra, N. G., Pestell, R. G., and Lisanti, M. P. (2003) Loss of caveolin-1 gene expression accelerates the development of dysplastic mammary lesions in tumor-prone transgenic mice, *Mol. Biol. Cell 14*, 1027−1042.
21. Capozza, F., Williams, T. M., Schubert, W., McClain, S., Bouzahzah, B., Sotgia, F., and Lisanti, M. P. (2003) Absence of caveolin-1 sensitizes mouse skin to carcinogen-induced epidermal hyperplasia and tumor formation, *Am. J. Pathol. 162*, 2029−2039.
22. Woodman, S. E., Cheung, M. W., Tarr, M., North, A. C., Schubert, W., Lagaud, G., Marks, C. B., Russell, R. G., Hassan, G. S., Factor, S. M., Christ, G. J., and Lisanti, M. P. (2004) Urogenital alterations in aged male caveolin-1 knockout mice, *J. Urol. 171*, 950−957.
23. Engelman, J. A., Chu, C., Lin, A., Jo, H., Ikezu, T., Okamoto, T., Kohtz, D. S., and Lisanti, M. P. (1998) Caveolin-mediated regulation of signaling along the p42/44 MAP kinase cascade in vivo. A role for the caveolin-scaffolding domain, *FEBS Lett. 428*, 205−211.
24. Couet, J., Sargiacomo, M., and Lisanti, M. P. (1997) Interaction of a receptor tyrosine kinase, EGF-R, with caveolins. Caveolin binding negatively regulates tyrosine and serine/threonine kinase activities, *J. Biol. Chem. 272*, 30429−30438.
25. Galbiati, F., Volonté, D., Engelman, J. A., Watanabe, G., Burk, R., Pestell, R. G., and Lisanti, M. P. (1998) Targeted downregulation of caveolin-1 is sufficient to drive cell transformation and hyperactivate the p42/44 MAP kinase cascade, *EMBO J. 17*, 6633−6648.
26. Scheel, J., Srinivasan, J., Honnert, U., Henske, A., and Kurzchalia, T. V. (1999) Involvement of caveolin-1 in meiotic cell-cycle progression in *Caenorhabditis elegans*, *Nat. Cell Biol. 1*, 127−129.
27. Hulit, J., Bash, T., Fu, M., Galbiati, F., Albanese, C., Sage, D. R., Schlegel, A, Zhurinsky, J., Shtutman, M., Ben-Ze'ev, A., Lisanti, M. P., and Pestell, R. G. (2000) The cyclin D1 gene is transcriptionally repressed by caveolin-1, *J. Biol. Chem. 275*, 21203−21209.
28. Sherr, C. J., and Roberts, J. M. (1999) Inhibitors of mammalian G1 cyclin-dependent kinases, *Genes Dev. 13*, 1501−1512.
29. Kitagawa, M., Higashi, H., Jung, H. K., Sujuki-Takahashi, I., Ikeda, M., Tamai, K., Kato, J., Segawa, K., Yoshida, E., Nishimura, S., and Taya, Y. (1996) The consensus motif for phosphorylation by cyclin D1-Cdk4 is different from that for phosphorylation by cyclin A/E-Cdk2, *EMBO J. 15*, 7060−7069.
30. Cozar-Castellano, I., Takane, K. K., Bottino, R., Balamurugan, A. N., and Stewart, A. F. (2004) Induction of β-cell proliferation and retinoblastoma protein phosphorylation in rat and human islets using adenovirus-mediated transfer of cyclin-dependent kinase-4 and cyclin D1, *Diabetes 53*, 149−159.
31. O'Sullivan, M., Scott, S. D., McCarthy, N., Figg, N., Shapiro, L. M., Kirkpatrick, P., and Bennett, M. R. (2003) Differential cyclin E expression in human in-stent stenosis smooth muscle cells identifies targets for selective anti-restenosis therapy, *Cardiovasc. Res. 60*, 673−683.
32. Roy, J., Tran, P. K., Religa, P., Kazi, M., Henderson, B., Lundmark, K., and Hedin, U. (2002) Fibronectin promotes cell cycle entry in smooth muscle cells in primary culture, *Exp. Cell Res. 273*, 169−177.
33. Cho, K. A., Ryu, S. J., Park, J. S., Jang, I. S., Ahn, J. S., Kim, K. T., and Park, S. C. (2003) Senescent phenotype can be reversed by reduction of caveolin status, *J. Biol. Chem. 278*, 27789−27795.
34. Zhang, W., Razani, B., Altschuler, Y., Bouzahzah, B., Mostov, K. E., Pestell, R. G., and Lisanti, M..P. (2000) Caveolin-1 inhibits epidermal growth factor-stimulated lamellipod extension and cell migration in metastatic mammary adenocarcinoma cells (MTLn3). Transformation suppressor effects of adenovirus-mediated gene delivery of caveolin-1, *J. Biol. Chem. 275*, 20717−20725.

BI049609T